into Earth orbit is independent of launch vehicle size and equals the cost of every 4 kw installed into an electric upper stage, also independent of size. It is important to realize that neither payload cost nor the cost of an electric stage can be expected to be independent of size; the results obtained by means of this simplification can therefore not be of general validity. However, this simple-minded assumption will be found of considerable help in illustrating the method. A circular orbit around Jupiter with an altitude of 20 planetary radii is to be established. Under these conditions, the diagram shown in Fig. 4 may be constructed. As in the previous figures, the payload is plotted along the ordinate whereas the initial mass capability of the ballistic system is plotted along the bottom abscissa. In order to obtain the performance boundary for systems of equal cost, rather than systems of equal initial mass, the horizontal scale at the top of the diagram, which is determined by the tradeoff ratio, has been used for the performance of the hybrid vehicles. Under these conditions, along any vertical line ballistic and hybrid systems exhibit the same recurrent cost. For the hypothetical cost assumptions used in this Note, a hybrid system which equals the cost of a ballistic system must be based on a launch vehicle whose initial mass capability is approximately 48% of the initial mass capability of the ballistic counterpart, i.e., the tradeoff ratio is 0.48. Comparing Fig. 4 to Fig. 1, it becomes evident that the equal performance boundary has been modified by the inclusion of the equal cost groundrule. Specifically, the area of ballistic superior performance has been enlarged in such a way as to roughly double the magnitude of the payload maximum. The shaded line indicates the physical limit of capability for the ballistic system. Below this line, the ballistic system is capable of performing the mission but, outside the area B, requires more trip time than the hybrid system. To further aid in the comparison, the hybrid performance lines for the longest (1000 days) and shortest (600 days) ballistic trip times are also shown in the diagram as broken lines inside H, the area of superior hybrid performance.

Concluding Remarks

A method has been developed which allows one to compare the performances of space propulsion systems of widely differing characteristics. Biased comparisons can be avoided by systematically arranging and selecting the groundrules of the comparison before they are fed into the analysis. Meaningful results can be obtained in spite of the large range of uncertainties attached to some of the performance parameters by adopting the use of scaling laws which reflect major trends or other relationships of interest rather than scattered performance estimates. This Note has intentionally been limited to a description of the method. Quantitative conclusions may be obtained by exercising the use of realistic performance and cost inputs whenever available.

References

[1] Mascy, A. C., Dugan, D. W., and Pitts, S. W., "Applications of Combined Electric, High Thrust Propulsion Systems," *AIAA Journal of Spacecraft and Rockets*, Vol. 5, No. 7, July 1968, pp. 785–791.

[2] Pinkel, B. et al., "Electrical Propulsion in Space: Mission Comparisons, Development Cost, Reliability and Their Implications for Planning," NAS 8-11081, Contract NAS r-21, Aug. 1964, The RAND Corp.

[3] Mascy, A. C., "A Computer Program for Quickly Analyzing Electric Propulsion Missions," proposed NASA TN.

[4] "SNAP 8 Performance Potential Study," NASA CR-722 S4, 1967, Aerojet-General Corp.

[5] Brown, H. and Taylor, J., "Navigator Study of Electric Propulsion for Unmanned Scientific Missions," CR-565, 1966, NASA.

[6] "Mission Engineering Study of Electrically Propelled Manned Planetary Vehicles," ANSO Document 6300-213, Contract NAS 8-20372, May 1967, General Electric Co.

[7] "Unmanned Electric Propulsion Mission Capabilities of the SNAP 50/SPUR Powerplant," PWAC-447, Contract AT(30-1)-2789, Oct. 1964, Pratt and Whitney Aircraft, Div. of United Aircraft Corp.

[8] Mascy, A. C., "Low-Thrust Mission Simulation—Feedback to Hardware Definition," *7th Electric Propulsion Conference*, AIAA, New York, 1969.

Solubilities of Gases in Simple and Complex Propellants

E. T. Chang,* N. A. Gokcen,* and T. M. Poston*
Aerospace Corporation, El Segundo, Calif.

Nomenclature

A	=	constant defined by $\Delta H^0/4.5756$, see ΔG^0
B	=	constant defined by $\Delta S^0/4.5756$, see ΔG^0
ϵ/k	=	force constant in °K for gases obtained from an equation such as Lennard-Jones equation for potential energy vs intermolecular distance, and from the second virial coefficient
ΔG^0	=	change in standard Gibbs energy, $\Delta G^0 = \Delta H^0 - T\Delta S^0$, cal/mole
ΔH^0	=	change in standard enthalpy in calories per mole for dissolution process
i	=	solute, a sparingly dissolved gas in this Note
j	=	solvent, a propellant in this Note
K_i	=	equilibrium constant; mole fraction of solute i divided by its partial pressure P_i in atmospheres over solution
K_i(ppm)	=	concentration, ppm, of i in solution divided by its partial pressure P_i, atm, over solution
n	=	number of moles
P	=	pressure, atm
ppm	=	parts per million of concentration in weight
R	=	ideal gas constant; 0.0820537 liter-atm/°K-mole in $PV = RT$, and 1.987165 cal/°K-mole in $\Delta G^0 = -RT \ln K_i$
ΔS^0	=	change in standard entropy in calories/mole/°K
T	=	temperature, °K
V	=	volume, liter
X_i	=	mole fraction of i; for simple propellants in this paper $X_i + X_j = 1$
Z	=	compressibility factor, dimensionless

Introduction

LIQUID propellants are pressurized with gases for two main reasons: 1) to provide a protective blanket for the propellants, and 2) to eject the propellants from their containers in the space vehicles. This process eliminates the use of heavy pumps and increases the payload. The gases used for pressurization dissolve to various extents[1–3] and cause pressure decay in the containers. The pumps and the venturis desorb the gases in solution in the form of small bubbles and cause undesirable hydrodynamic effects. A knowledge of the solubilities of gases in liquid propellants is therefore very useful.

Experimental Procedure

The apparatus for solubility measurements, shown in Fig. 1, was all Pyrex glass construction with short capillary connecting tubes joined by fusion. Two capillary stopcocks A and B were sparingly lubricated with silicone grease. Three volumes C, D, and E, calibrated to ±0.0003 mliter, were interconnected with short capillary necks, each with a calibration mark. These volumes were immersed in a

Received May 23, 1969.

* Member of Chemical Thermodynamics Section, Laboratories Division.

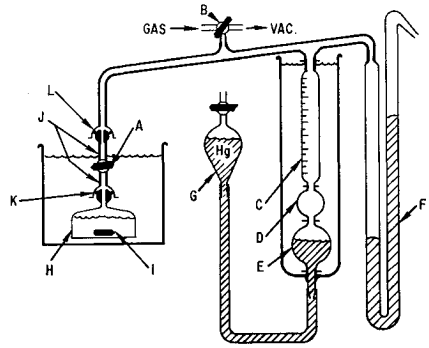

Fig. 1 Apparatus.

thermostat whose temperature was very nearly the same as the thermostated room where the apparatus was located. A precision manometer F, accurate to ±0.01 mm, was read with a microslide cathetometer. The volume of a gas in the calibrated volumes C, D, and E, was changed either by adjusting the vertical position of a levelling bulb G filled with mercury and attached to E with a reinforced flexible tygon tubing, or by pressurizing G with a compressed gas connected to the stopcock above G. The propellant bulb H was of 3-in. o.d. and 1 in. high with a capacity of about 100 mliter; it was calibrated with an accuracy of ±0.0002 mliter by using water or mercury. The bulb H was designed to have about 5 mliter space, or ullage, above the fully exposed liquid surface. A glass enclosed magnet bar I, activated with an externally rotating magnetic field at 200 rpm was used for stirring the propellant in H. A short capillary connector J with a specially designed O-ring joint K was attached to H. A second O-ring joint L was used for attaching the connector I to the rest of the apparatus. The volume of connector I, above and below the stopcock A, was calibrated by mercury displacement. All the interconnecting capillary volumes and the volume above the mercury in the manometer were calibrated to ±0.0003 mliter accuracy by using nitrogen at two pressures. The propellant bulb H was immersed in a thermostat controlled to ±0.01°C. The atmospheric pressure was read with a special barometer accurate to ±0.02 mm.

The measurements of gas solubility were made as follows. The bulb and the connector were assembled and evacuated, the stopcock A was closed, the connector-bulb assembly was detached at L from the apparatus and weighed on an analytical balance. If a simple propellant or a simple binary or ternary mixture was to be used in the experiment, it was distilled into the bulb and then the connector-bulb assembly was reweighed to obtain the weight of the propellant. If the propellant was complex, such as a ramjet fuel, or the fuming nitric acid, it was placed directly into the bulb with a syringe and degassed at sufficiently low temperatures to prevent a loss of weight more than 0.1 gram in order to preserve the composition of propellant. The calibrated volumes and connections were evacuated and thoroughly flushed with the desired gas by using the stopcock B, after the bulb-connector assembly was attached to the apparatus. The bulb was immersed into the thermostat to start the measurements. The gas whose solubility was to be measured was admitted into the calibrated volumes through B and its amount was obtained by measuring P, V, and T and by using the gas law $PV = nZRT$. The gas was forced over the propellant by using the levelling bulb after opening the stopcock A on the connector. The dissolution process requires less than 10 min when the propellant was vigorously stirred with the magnet bar, but 40 min were allowed to assure that there was no further changes in pressure readings. The measurements of P, V, T of the gas above the propellant, and P, V, T of the remaining gas beyond the stopcock A in the connector after A had been turned off and the gas had been expanded or compressed to a convenient calibration point, yielded the remaining or undissolved gas. The dissolved gas was the difference between the initially admitted gas and the remaining gas. The calculation of remaining gas over the propellant required highly precise measurements of the vapor pressure of each propellant[4] and its density[5] in a separate apparatus.

The accuracy of experimental procedure was checked by measuring the solubility of nitrogen in water. The results agreed within 2% of the well-established available data.[6]

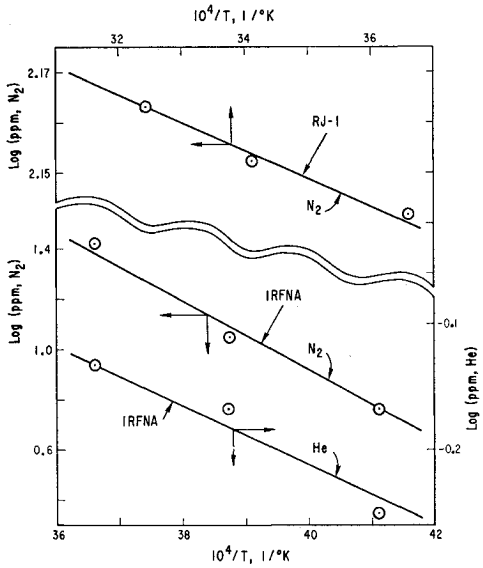

Fig. 2 Solubilities of gases in RJ-1 and IRFNA as functions of temperature.

Results

The solubility in terms of the concentration of a dissolved gas i, e.g., in mole fraction X_i, is proportional to the partial pressure P_i in accordance with Henry's law. This can be demonstrated either by plotting X_i vs P_i or by the constancy of the equilibrium constant $K_i = X_i/P_i$ for the fol-

Table 1 Solubilities of gases in propellants. Values of A and B for Eq. (5) and atmospheric solubilities at 0° and 25°C

Gas	Propellant	A	B	Solubility at 1 atm ppm, 0°C	ppm, 25°C
He	N_2O_4	−521	2.3874	3.0	4.3
N_2	N_2O_4	−153	2.8194	182	203
O_2	N_2O_4	−145	3.0367	320	355
Ar	N_2O_4	−104	2.9757	394	424
N_2O_3	N_2O_4	+1978	−0.3707	74,300[a]	62,600[a]
He	N_2H_4	−275	0.7387	0.5₄	0.6₅
N_2	N_2H_4	−516	2.5322	4.4	6.3
Ar	N_2H_4	−446	2.6841	11.3	15.4
He	MH[b]	−393	1.6586	1.6₅	2.1₈
N_2	MH	−245	2.5691	47	56
Ar	MH	−142	2.6664	140	155
He	SDMH[b]	−544	3.1409	14.1	20.7
N_2	SDMH	−284	3.8088	587	718
Ar	SDMH	−157	3.8448	1856	2075
He	UDMH[b]	−461	2.3410	4.5	6.2
N_2	UDMH	−175	2.8275	154	174
Ar	UDMH	−52	2.8351	440	456
He	Aerozine-50[b]	−443	1.8319	1.62	2.22
N_2	Aerozine-50	−257	2.5130	37	45
Ar	Aerozine-50	−169	2.6365	104	117
He	IRFNA	−232	0.7121	0.7₃	0.8₆
N_2	IRFNA	−1364	6.3730	24.0	62.8
CO_2	IRFNA[c]	+787	1.241	1.33×10^4	7.60×10^3
N_2	RJ-1	−56	2.3445	138	144
He	RJ-1[c]	−216	1.215	2.7	3.1

[a] Since the boiling point of N_2O_3 is about +3.5°C, the solubility for N_2O_3 has been calculated at 0.01 atm where it should obey Henry's law. All other values refer to 1 atm.

[b] MH = methyl hydrazine; SDMH = symmetrical dimethyl hydrazine; UDMH = unsymmetrical dimethyl hydrazine; Aerozine-50 = 50/50 mixture of N_2H_4 and UDMH.

[c] Estimated closely by using available data for other similar systems.

lowing reaction:

$$\text{gas } i = \text{dissolved } i \tag{1}$$

The dissolved i is called the solute, and the propellant j, the solvent. The calculation of X_i requires molecular composition of the liquid which is not always simple for substances such as kerosene, but the composition in weight percentage (%) or in ppm poses no particular difficulty. Further, % or ppm are related to the mole fraction by a simple factor

$$(100M_i/M_j)X_i = (\%i),\ 1 \text{ ppm} = 0.0001\% \tag{2}$$

where M_i and M_j are the molecular weights of i and j, respectively. Hence, the equilibrium constant K_i (ppm) in terms of ppm is given by

$$K_i = (\text{ppm}_i)/P = 10^6 M_i X_i / M_j P_i \tag{3}$$

Thus Henry's law is obeyed for dilute solutions irrespective of the units used in expressing the concentration of a dissolved gas.

The equilibrium constant K_i(ppm) for reaction (1) is related to the change in standard Gibbs energy (formerly called the Gibbs free energy) by the well-known thermodynamic relation[7]

$$\Delta G_i^0(\text{ppm}) = \Delta H_i^0 - T\Delta S_i^0 = -RT \ln K_i(\text{ppm}) \tag{4}$$

where ΔH_i^0 is the standard enthalpy change and ΔS_i^0 is the standard entropy change, both of which are virtually independent of temperature in the usual limited range of interest. The difference between ΔG_i^0 for ppm and ΔG_i^0 for X_i appears as a constant term in ΔS^0. A plot of log K_i vs $1/T$ gives a linear correlation of data represented by

$$\log K_i = A/T + B \tag{5}$$

where $A = -\Delta H^0/4.5756$ and $B = \Delta S^0/4.5756$.

The composition of inhibited red fuming nitric acid (IRFNA) is about 84% HNO_3, 14% N_2O_4, and the balance is equally divided between H_2O and HF. The composition of RJ-1 (kerosene rocket fuel) varies only slightly from one supplier to another over several years as judged from very small variations in highly precise data on the density of several batches. The data on solubilities are summarized in Table 1. The logarithm of the average value of K_i (ppm), which is also the atmospheric solubility for N_2 and He in IRFNA, and N_2 in RJ-1, are plotted vs $1/T$ in Fig. 2. The linear plots represent ΔG_i^0 (ppm) $= -RT \ln K_i$(ppm) for each gas, i.e.,

$$\Delta G_{He}^0(\text{ppm, IRFNA}) = 1060 - 3.26T \tag{6}$$

$$\Delta G_{N_2}(\text{ppm, IRFNA}) = 6240 - 29.16T \tag{7}$$

$$\Delta G_{N_2}(\text{ppm, RJ-1}) = 256 - 10.73T \tag{8}$$

The validity of Henry's law is shown clearly in Fig. 3 where it is evident that the concentration of N_2 varies linearly with the pressure of N_2 and the slope of the line is simply K_{N_2} (ppm, RJ-1) at 35°C.

Estimation of Solubilities

We have estimated the solubilities of CO_2 in IRFNA and He in RJ-1 by using the method of Hildebrand and Scott.[8] For this purpose we have used the compiled solubility data[6,10] for similar systems and ϵ/k for each gas from Hirschfelder, Curtiss, and Bird.[9] The values of ϵ/k, the force constants in °K, were obtained[9] by using the second virial coefficient for gases and a potential function such as the Lennard-Jones potential, which gives the potential energy as a function of distance of approach between two molecules. When log K_i is plotted vs ϵ/k, a straight line is obtained for each liquid solvent at a chosen temperature. To obtain the

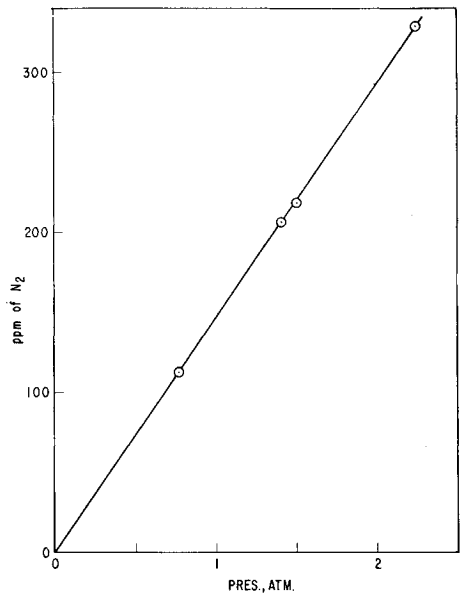

Fig. 3 Solubility of nitrogen in RJ-1 at 35°C.

solubility of CO_2 in IRFNA, logK_i (ppm) at 25°C for He and CO_2 in liquid N_2O_4, and N_2 and CO_2 in acetic acid were plotted, and the straight lines for the two solvents were drawn. The point for He in IRFNA was plotted and a line passing through this point was drawn so that it was proportionally distant from the two previous lines at increasing values of ϵ/k. The point on the line for IRFNA at ϵ/k for CO_2 gave logK_{CO_2} (ppm, IRFNA) at 25°C. This procedure was repeated at 0°C to obtain logK_{CO_2} (ppm, IRFNA) at 0°C. The substitution of the values of logK_{CO_2} (ppm, IRFNA) in $\Delta G^0 = -RT \ln K_i = \Delta H^0 - T\Delta S^0$ gave two simultaneous equations for obtaining ΔH^0 and ΔS^0. The result is

$$\Delta G_{CO_2}^0(\text{ppm, IRFNA}) = -3600 - 5.68T \tag{9}$$

The solubility of He in RJ-1 was estimated in the same manner by using the compiled data[6,10] for He and N_2 in hexane, He and N_2 in benzene, and H_2 and O_2 in kerosene and comparing the results with our data for N_2 in RJ-1. The resulting relationship is

$$\Delta G_{He}^0(\text{ppm, RJ-1}) = 990 - 5.56T \tag{10}$$

The values of atmospheric solubility from Eqs. (9) and (10) are listed in Table 1.

The equilibrium concentrations of dissolved gases in this Note are useful in obtaining the maximum amounts of gases dissolved when the propellant is pressurized. In actual practice the attainment of equilibrium takes a fairly long time under static conditions. For example it was shown by the authors[11] that the rate of dissolution of N_2 in liquid N_2O_4 varies exponentially with time. Mechanical agitation of the liquid increases the rate of solution of gases by several orders of magnitude. It is usually preferable to select a pressurization gas that is the least soluble in a given propellant. The results summarized in Table 1 show that helium should be used for pressurization in all cases when it is economically feasible.

References

[1] Chang, E. T. and Gokcen, N. A., "Solubilities of N_2, He, and Ar in Liquid N_2O_4," Rept. ATN-64(9228)-4, 1964, Aerospace Corp., El Segundo, Calif.

[2] Chang, E. T., Gokcen, N. A., and Robison, C. D., "Solubilities of O_2, NO and N_2O_3 in Liquid N_2O_4," Rept. TDR-469(5210-10)-6, 1965, Aerospace Corp., El Segundo, Calif.

[3] Chang, E. T., Gokcen, N. A., and Poston, T. M., "Solubilities of He, N_2 and Ar in Hydrazine and Unsymmetrical Dimethyl-

hydrazine," Rept. TR-0158(3210-10)-2, 1967, Aerospace Corp., El Segundo, Calif.

[4] Chang, E. T. and Gokcen, N. A., "Equilibria in N_2H_4-1, 1-$N_2H_2(CH_3)_2$ and He(or N_2)-N_2H_4-1, 1-$N_2H_2(CH_3)_2$ Systems," *Journal of Physical Chemistry*, Vol. 72, 1968, pp. 2556–2562.

[5] Kemppinen, A. I. and Gokcen, N. A., "Density of Dibutyl Phthalate," *Journal of Physical Chemistry*, Vol. 60, 1956, pp. 126–127.

[6] Seidell, A. and Linke, W. F., *Solubilities of Inorganic and Metal Organic Compounds*, Van Nostrand, New York, 1958.

[7] Penner, S. S., *Chemistry Problems in Jet Propulsion*, Pergamon Press, New York, 1957, Ch. XII.

[8] Hildebrand, J. H. and Scott, R. L., *Regular Solutions*, Prentice-Hall, Englewood Cliffs, N.J., 1962, p. 47.

[9] Hirschfelder, J. O., Curtiss, C. F., and Bird, R. B., *Molecular Theory of Gases and Liquids*, Wiley, New York, 1964, pp. 156, 191, and 195; also p. 44 in Ref. 8.

[10] Stephen, H. and Stephen, T., eds., *Solubilities of Inorganic and Organic Compounds*, MacMillan, New York, 1963.

[11] Chang, E. T. and Gokcen, N. A., "Rate of Solution of N_2 in Liquid N_2O_4," Rept. TR-1001 (2210-10)-1, 1966, Aerospace Corp., El Segundo, Calif.

Graphically Determining Sounding Rocket Vehicle Attitudes

CHARLES F. MILLER JR.*
Goddard Space Flight Center, Greenbelt, Md.

COORDINATES used to determine the attitude of a sounding rocket vehicle are commonly derived from the solar or lunar aspect angle, designated α, in association with the magnetic aspect angle, designated θ, which is the angle of the rocket's longitudinal axis with respect to the local magnetic field vector. On sounding rockets, optical sensors measure α once each spin cycle, and a flux-gate magnetometer measures θ. The angle between α and θ, designated the phase angle ϕ, is measurable from telemetry records. Sun and magnetic south point positions are plotted; then α and θ are used to determine the azimuth and zenith distance of the rocket's longitudinal axis. When the time sequence of rocket positions in flight has been plotted, the momentum vector can be determined. With any known rocket position, any other portion of the sky can be mapped for that orientation, using coordinate transformation.

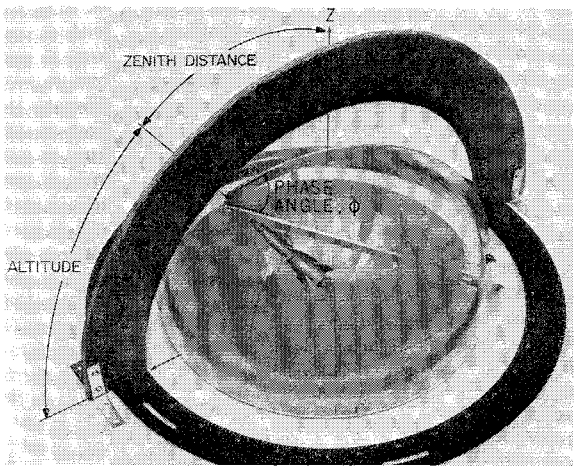

Fig. 1 Aspect-angle protractors aligned with sun and magnetic south point, and generating phase angle at the rocket.

Figure 1 depicts the three-dimensional parameters. The altitude A of the rocket is the number of degrees (0–90) on the vertical circle from the horizon to the axis of the rocket. The zenith distance is the angle between the zenith Z, directly over the center of gravity of the rocket, and the longitudinal axis of the vehicle. The zenith distance is the complement of the altitude and, in this discussion, is represented by the arc at a fixed radius from the origin. The sky is represented by a spherical shell on which lines of altitude and azimuth are plotted every 10°. The rocket's attitude is the combination of its altitude and its azimuth. On this shell, the position of the vehicle's nose, or the position of any celestial body, can be plotted. The rocket's center of mass locates the center of the base of the plastic hemisphere; from that point α, θ, and ϕ are measured. In Fig. 1, a hinged protractor, concentric with the rocket's center of mass, is situated with the hinge aligned with the rocket's longitudinal axis, one leg in the plane of the incident sunlight, and the other in the plane of the magnetic flux vector, i.e., over the south magnetic point. The phase angle ϕ can be measured between the protractor's two halves and can be seen to be the dihedral angle between two planes, one made by the angle of the sun's rays with the rocket's longitudinal axis and the other made by the angle of the local magnetic flux vector with that axis.

Figure 2 is a zenith view of the same situation, with black arcs defining α and θ. From the magnetic south point to the sun, a black arc completes the spherical triangle used to determine the zenith distance and azimuth of the vehicle's nose. As a step toward reducing the three-dimensional system to two dimensions, Fig. 2 was taken directly over the zenith. Thus, the view represents the projection of the horizon system down to the plane of the horizon. The altitude is a cosine function of the radius from Z, thus the first 15° of altitude are hardly separable in the photograph.

Reduction to Polar Coordinates

To transform spherical parameters to two coordinates, a plot is made on polar graph paper of the sky from the horizon to the zenith. In Fig. 3, such a plot has been made of the situation depicted in Fig. 2. In Fig. 3, any radius is an azimuth angle R with reference to north, and increments along a chosen radius mark either the altitude or its complement, the zenith distance. The time, latitude β, and longitude λ of the rocket flight are required for the location of the sun on polar graph paper. For Nike-Apache shots, an average solar position is within the required accuracy, but for longer and higher flights, the trajectory should be divided into parts, and each successive time interval should specify β and λ to

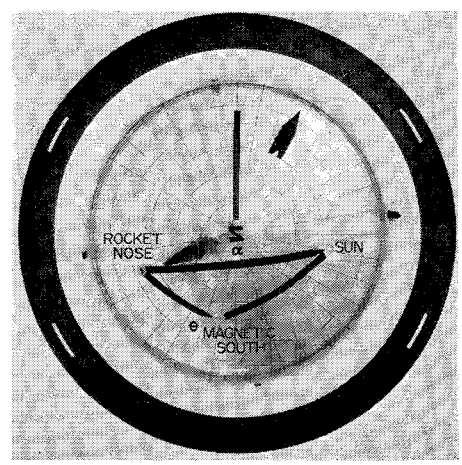

Fig. 2 Zenith view of Fig. 1, showing spherical triangle.

Received April 15, 1969; revision received August 1, 1969.
* Aerospace Technologist. Member AIAA.